ELSEVIER

Journal of Structural Geology 26 (2004) 1195–1214

JOURNAL OF STRUCTURAL GEOLOGY

www.elsevier.com/locate/jsg

The impact of the linkage between grade distribution and petrofabric on the understanding of structurally controlled mineral deposits: Ouro Fino Gold Mine, Brazil

R.N. Monteiro[a,*], W.S. Fyfe[b], F. Chemale Jr[c]

[a]*Inco Technical Services Limited, Copper Cliff, Ontario, Canada*
[b]*Department of Earth Sciences, The University of Western Ontario, London, Ontario, Canada*
[c]*Isotope Geology Laboratory, Rio Grande do Sul University, Porto Alegre, RS, Brazil*

Received 21 November 2002; received in revised form 1 September 2003; accepted 18 September 2003

Abstract

Ore deposit structural analysis, using a combination of structural geology and geostatistics, has direct application in the mining industry. Its main goal is to integrate structural measurements and assay data to create a method in which structurally controlled deposits are modeled numerically. This provides guidance to grade control and pit optimization during mining, improves prediction of orebody geometry and orientation, and provides more effective exploration strategies for surrounding areas. The method leads to a better understanding of how mineralized fluids percolated and were focused at the Ouro Fino Mine, a shear zone-hosted gold deposit in Minas Gerais State, Brazil. In this mine, gold is distributed along permeability pathways within rock fabrics that were produced or modified during the Brasiliano orogeny, when the Espinhaço–Araçuaí sequence was inverted towards the São Francisco craton during a basement-involved fold-and-thrust regime. The resulting permeable zones are conformable with the C surface, within which two other clusters of fabric elements control the large-scale features of the mineralization: (1) a cluster of fabric elements (mineral, stretching and intersection lineations) that plunges SE; and (2) a sub-horizontal cluster along folds and intersection lineations and the strike of the shear zone.

Keywords: Structure; Geostatistics; Ore deposit structural analysis; Ouro Fino Mine; Brazil

1. Introduction

Predictions of shape, orientation and distribution of mineral deposits and individual ore shoots, both on a local scale and regionally, present fundamental challenges to the mining industry because the success of exploration programs and mining operations is greatly influenced by the accuracy of these predictions.

Ore deposit structural analysis relies on two assumptions; viz: (1) tectonic processes create and modify the architecture of mineral deposits and, in cases where mineralization is controlled by the structure, there must be a linkage between structure and grade distribution; and (2) mapping and structural analysis of mineral deposits provide the characterization and spatial orientation of structural objects, and geostatistics tells us about the grade distribution. If grade and structure are related, then it should be possible to estimate this relationship by combining tools from both fields, provided they are both applied within the same structural domain.

This paper looks at the relationships between structure and gold mineralization in the Ouro Fino Mine, Minas Gerais State, Brazil. It explores the linkage between structural geology and geostatistics following an approach described by Monteiro (1996).

2. Regional and local geology

The Ouro Fino Gold Mine is located 14 km southwest of the Town of Riacho dos Machados, in the north part of Minas Gerais State, Brazil, about 560 km northeast of the State Capital, Belo Horizonte. The mine is situated near the eastern margin of the São Francisco Craton, which is a tectonic unit affected by the Brasiliano–Pan-African event (Neoproterozoic to Eopaleozoic, herein denominated Brasiliano) (Fig. 1a). In terms of lithostratigraphic units, the

* Corresponding author. Tel: +1-705-682-8243; fax: +1-705-682-8422.
E-mail address: monteiror@inco.com (R.N. Monteiro).

0191-8141/$ - see front matter © 2004 Elsevier Ltd. All rights reserved.
doi:10.1016/j.jsg.2003.11.023

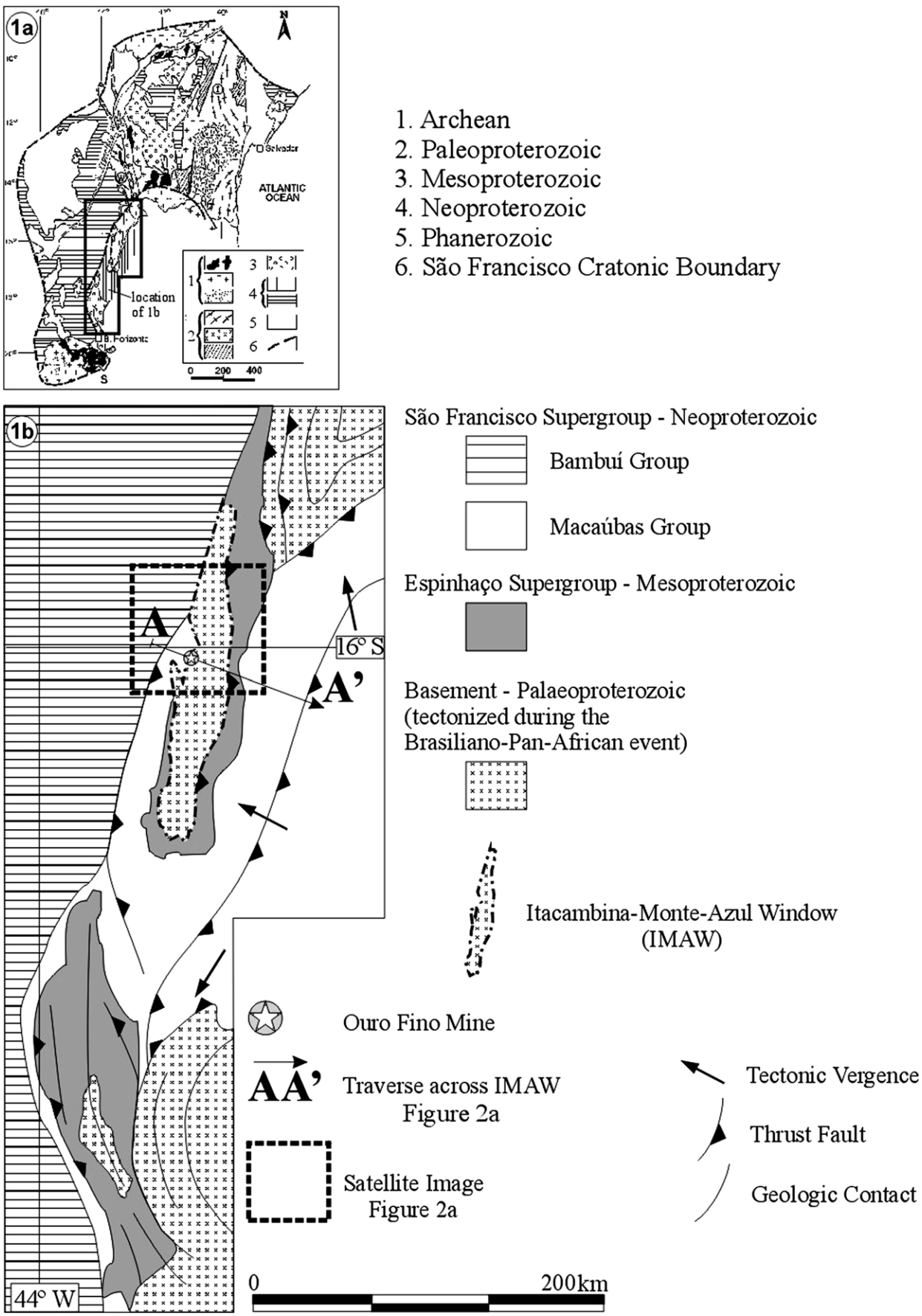
1a
N
Salvador
ATLANTIC OCEAN
location of 1b
B. Horizonte
S
1
2
3
4
5
6
0 200 400
1. Archean
2. Paleoproterozoic
3. Mesoproterozoic
4. Neoproterozoic
5. Phanerozoic
6. São Francisco Cratonic Boundary
1b
A
A'
16° S
São Francisco Supergroup - Neoproterozoic
Bambuí Group
Macaúbas Group
Espinhaço Supergroup - Mesoproterozoic
Basement - Palaeoproterozoic
(tectonized during the
Brasiliano-Pan-African event)
Itacambina-Monte-Azul Window
(IMAW)
Ouro Fino Mine
AA'
Traverse across IMAW
Figure 2a
Satellite Image
Figure 2a
Tectonic Vergence
Thrust Fault
Geologic Contact
44° W
0
200km

region is made up of Palaeoproterozoic granite–gneisses and amphibolites, Mesoproterozoic Espinhaço Supergroup units (continental rift-related rocks and shallow-water marine sequences), Neoproterozoic glacial units of the Macaúbas Group, Neoproterozoic shallow-water, carbonate-bearing Bambuí Group (Fig. 1b) and Brasiliano granites. The Ouro Fino mine occurs in a shear zone hosted in the Palaeproterozoic unit within the Itacambira–Monte Azul Window (IMAW) (Fig. 1b). Based on LandSat image interpretation and regional traverses we distinguished three main tectonic domains, from east to west: (1) Espinhaço–Araçuaí fold and thrust belt (EAFTB), (2) Itacambira–Monte Azul window (IMAW), and (3) São Francisco Craton (Fig. 2a and b). Fig. 3 is a schematic representation of the recognized tectonic events and units for the region in which the study area is located.

The EAFTB and SFC comprise Mesoproterozoic and Neoproterozoic rocks that are the cover sequence that surrounds the IMAW. All units are affected by the westward Brasiliano event so the magnitude of deformation diminishes from west to east, as we observed in the traverse of Fig. 2b. The tectonic displacement recorded for the cover rocks during the westward Brasiliano orogeny formed subhorizontal detachments with connected thrusting, strike-slip transfer zones and associated folding (Monteiro, 1996) as already described in regional works for the EAFTB (Marshak and Alkimin, 1989; Uhlein et al., 1992; Chemale et al., 1993). Basement-involved tectonism during the Brasiliano created the regional and local setting for the study area (Monteiro, 1996).

The Espinhaço–Araçuaí fold-and-thrust belt has a strong foliation with stretching lineations and kinematic features indicating tectonic transport toward the São Francisco Craton (Marshak and Alkimin, 1989; Chemale et al., 1993). The distal area to the craton has a down-dip stretching lineation in rocks at the amphibolite facies. Both the rake of this structural element and the metamorphic grade decrease toward the cratonic area. The area proximal to the craton features strike-slip faults and thrust faults with frontal and oblique ramps (Pedrosa-Soares et al., 1992a). The mineral lineation for the cover plunges about 45° towards 120–130° (Belo, 1994a,b).

2.1. Itacambira–Monte Azul Window

North–south elongated basement windows are common features within the Espinhaço–Araçuaí fold-and-thrust belt, and the Itacambira–Monte Azul window, a 30-km-wide and 100-km-long basement structure, is one of these features (Fig. 1a and b). Guimarães et al. (1993) recognized six stratigraphic units within the IMAW: (1) Córrego do Cedro Metamorphic Complex; (2) Riacho dos Machados Metamorphic Suite (Fonseca, 1993; Monteiro, 1996); (3) Pedra do Urubu Granitic Suite; (4) Gorutuba Granitic Suite; (5) Paciência Monzonitic Suite; and (6) Confisco Granitic Suite. The last two units are Brasiliano age intrusives.

Our interest focuses on the Riacho dos Machados Metamorphic Suite, which represents the host unit to the shear zone where the Ouro Fino mine is located. The Riacho dos Machados Metamorphic Suite includes amphibolite-grade ortho- and para-metamorphic rocks, such as metabasic rocks, garnet–biotite, quartzo-feldspathic, and mafic schists and gneisses. Belo (1994a,b) describe the Ouro Fino Mine Shear Zone as part of a larger system of shear zones that disrupt rocks of the Córrego do Cedro Metamorphic Complex, Pedra do Urubu Granitic Suite, Gorutuba Granitic Suite and Riacho dos Machados Metamorphic Suite units.

Ages of the basement units within the Itacambira–Monte Azul Window are not well constrained. Some whole rock and mineral Rb/Sr and Pb/Pb geochronologic data yielded an Archean age of 2780 ± 130 Ma with an overprint between 2.0 and 1.8 Ga (Siga et al., 1987a,b), which lead them to suggest that there was an important metamorphic reworking during the Paleoproterozoic. The basement complex also intruded by granites formed at 574 ± 10 to 670 ± 18 Ma (Siga et al., 1987b) and 512 ± 5 Ma U/Pb (zircon overgrowth) (Machado et al., 1989). Guimarães et al. (1993) suggested a Paleoproterozoic origin for the Riacho dos Machados Metamorphic Suite, with subsequent metamorphism, based on the geochronological events present in the IMAW, along with structural analysis. Formation of the Pedra do Urubu Granitic Suite and Gorutuba Granitic Suite has been assigned to the same period. These authors also suggest that the intrusion of the Paciência Monzonitic Suite and Confisco Granitic Suite occurred pre- or syn-Brasiliano orogeny.

2.2. Fold-and-thrust sequence

The Mesoproterozoic to Neoproterozoic cover sequence that constitutes the EAFTB is composed of two supergroups: the Espinhaço and the São Francisco (Fig. 1b). The 3000-m-thick Espinhaço Supergroup includes continental and transitional marine sedimentary sequences (Schöll and Fogaça, 1979; Marshak and Alkimin, 1989). The geological contacts with the São Francisco Supergroup are gradational, erosional or tectonic (Pflug and Renger, 1973; Magalhães, 1988; Marshak and Alkimin, 1989). The 900-m-thick São Francisco Supergroup is subdivided into the Macaúbas Group, of glacial origin, and the Bambuí Group, which overlies it. The Bambuí Group is composed of a basal shallow-water marine sedimentary sequence, overlain by sandstones and shales from a fluvial, shallow-water marine

Fig. 1. Geological sketch of the study region (a) the São Francisco Craton and its eastern belts (Mascarenhas et al., 1984); and (b) the regional map of Itacambira–Monte Azul region with the location of the study area (modified from Pedrosa-Soares et al. (1992a)).

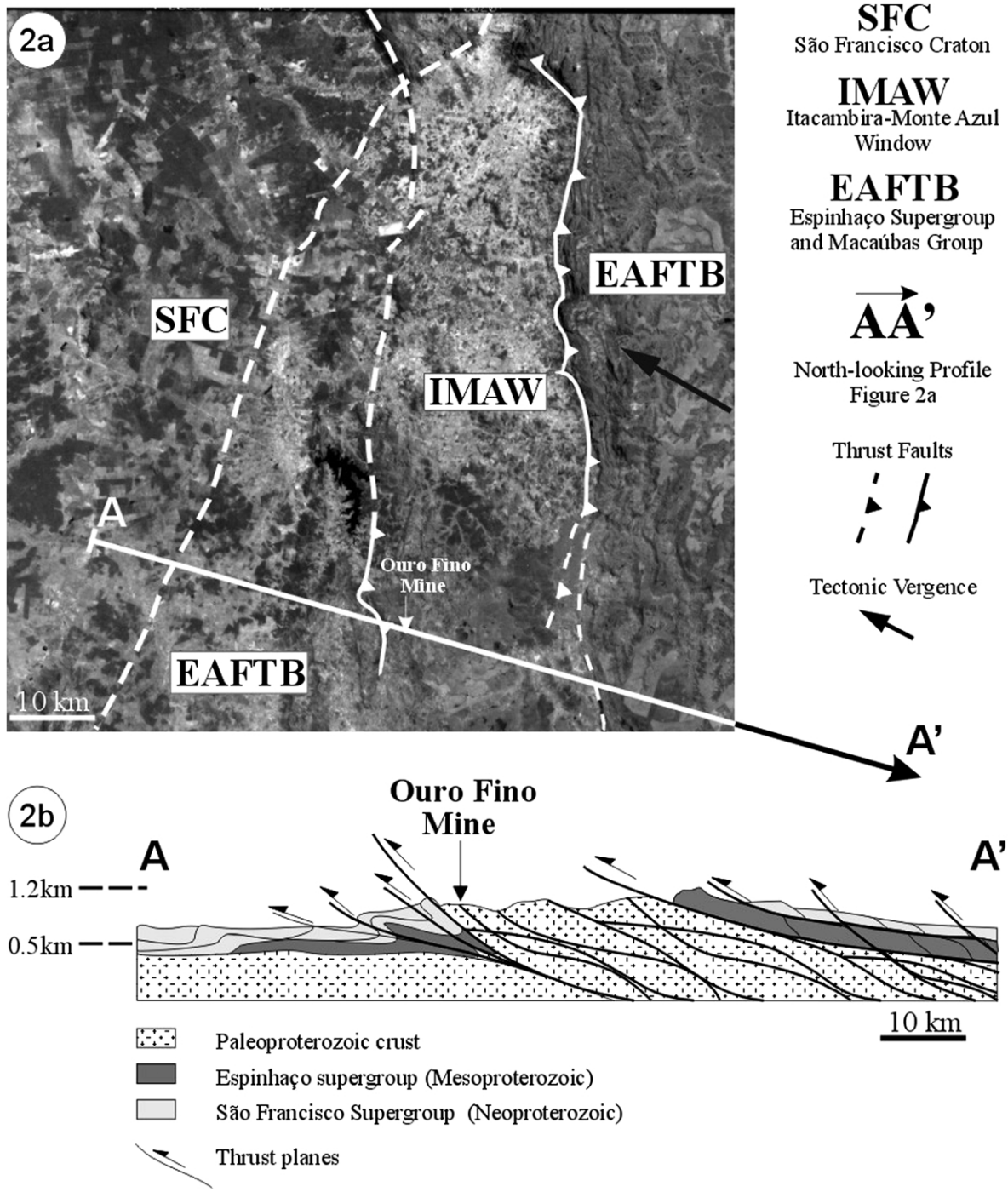

Fig. 2. Satellite image and regional traverse. (a) The three main lithotectonic domains of the study area: the São Francisco Craton (SFC), the Itacambira–Monte Azul Window (IMAW), and the Espinhaço–Araçaí Fold-and-Thrust Belt (EAFTB). (b) The NW–SE-trending traverse along the study area showing the main tectonic relationships (modified from Pedrosa-Soares et al. (1992a)). The IMAW is herein interpreted as Paleoproterozoic Crust re-worked during the Brasiliano tectonic event.

environment (Kiang et al., 1988; Marshak and Alkimin, 1989). Geochronological data available for the sequence indicates that sedimentation of the Espinhaço Supergroup began between 1844 ± 15 and 1715 ± 2 Ma and terminated around 906 ± 2 Ma (Machado et al., 1989). The age of the São Francisco Supergroup sedimentation is still the subject of debate; however, it is limited by 906 ± 2 Ma and the Brasiliano Orogeny (started around 700–600 Ma ago). Structural and geochronological comparisons between the Espinhaço and the São Francisco Supergroups indicate a single compressive event during the Brasiliano Orogeny. The cover sequence shows a decreasing degree of deformation from east to west, with no ductile deformation over the cratonic area (Machado et al., 1989; Marshak and

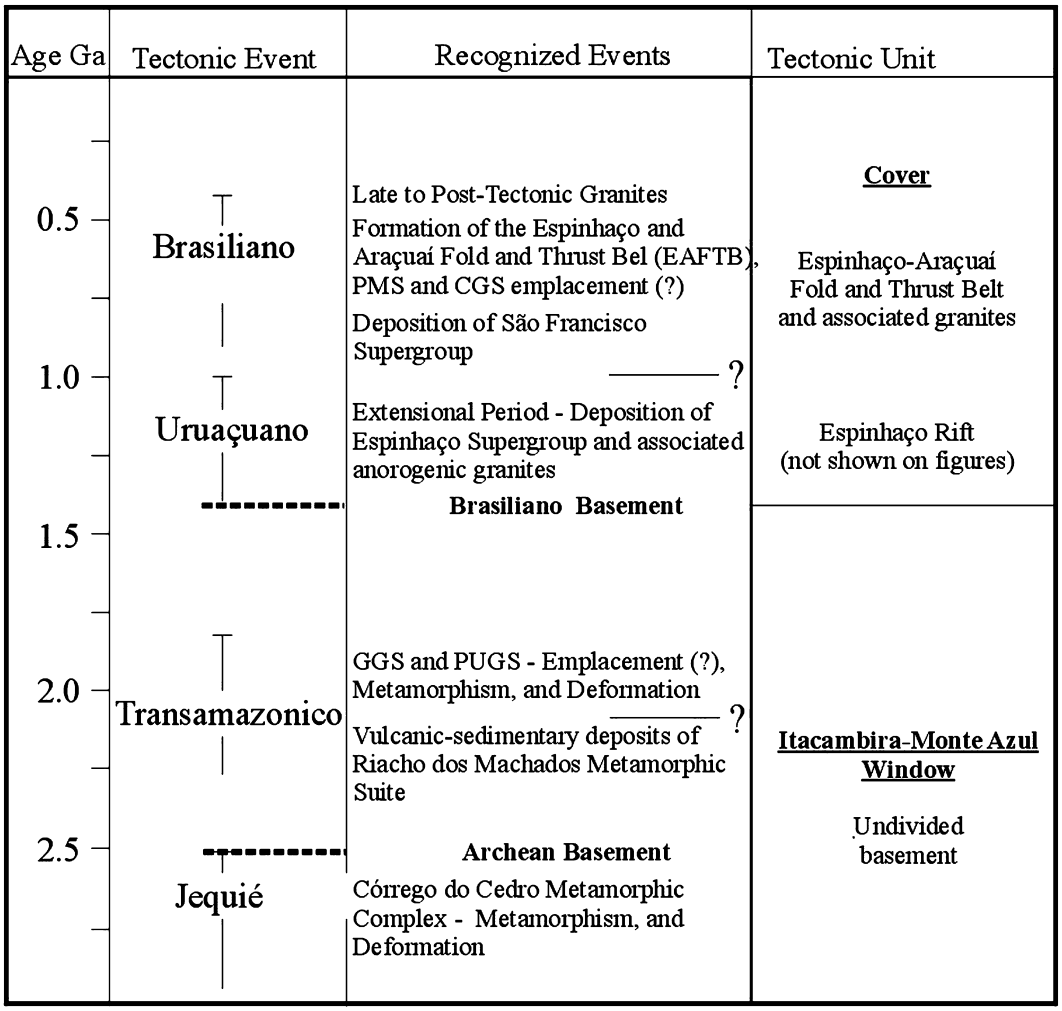

Fig. 3. Schematic representation of the recognized tectonic events and units for the area under investigation—see text for explanation (after Siga et al., 1987a,b; Machado et al., 1989; Marshak and Alkimin, 1989; Pedrosa-Soares et al., 1992b; Guimarães et al., 1993; Chemale et al., 1994). PMS, CGS, GGS and PUGS are Paciência Monzonitic Suite, Confisco Granitic Suite, Gorutuba Granitic Suite, and Pedra do Urubu Granitic Suite, respectively.

Alkimin, 1989; Pedrosa-Soares et al., 1992a; Chemale et al., 1994).

2.3. Tectonic evolution of basement and cover sequence

Four major tectonic events molded the area under investigation The IMAW basement rocks were formed and metamorphosed during the Archean and Paleoproterozoic events. Early development of the cover sequence started with northward intracontinental rifting at 1.7 Ga and finished with the deposition of the Espinhaço Supergroup (Marshak and Alkimin, 1989). A new depositional cycle started at 1.0 Ga with the formation of the Macaúbas glacial deposits. Subsequently, the Espinhaço–Araçuaí fold-and-thrust belt reactivated basement rocks in particular zones of the IMAW during the Brasiliano Orogeny in a basement-involved tectonism (Marshak and Alkimin, 1989; Chemale et al., 1993). Inversion tectonics initiated at 700–600 Ma (Almeida, 1977), when the Espinhaço Supergroup and the Macaúbas Group were thrust toward the São Francisco craton, and downwarping of the lithosphere at the cratonic margin created the foreland basin of the upper São Francisco Supergroup (Kiang et al., 1988).

2.4. Ouro Fino Mine geology

The Ouro Fino Mine is hosted in a 1400-m-long by 200-m-wide shear zone (Figs. 1b, 2a and b and 4). The contacts of this zone with the Riacho dos Machados Metamorphic Suite are thrust faults dipping between 30 and 40° toward 115° (Belo, 1992 in Fonseca, 1993). Locally, biotite schists and biotite gneisses are the most prominent rock types of the metamorphic suite, in which kyanite, staurolite, garnet and plagioclase, together with biotite and quartz, make up the main mineral assemblage. The biotite schist and biotite gneiss rocks develop a distinctive

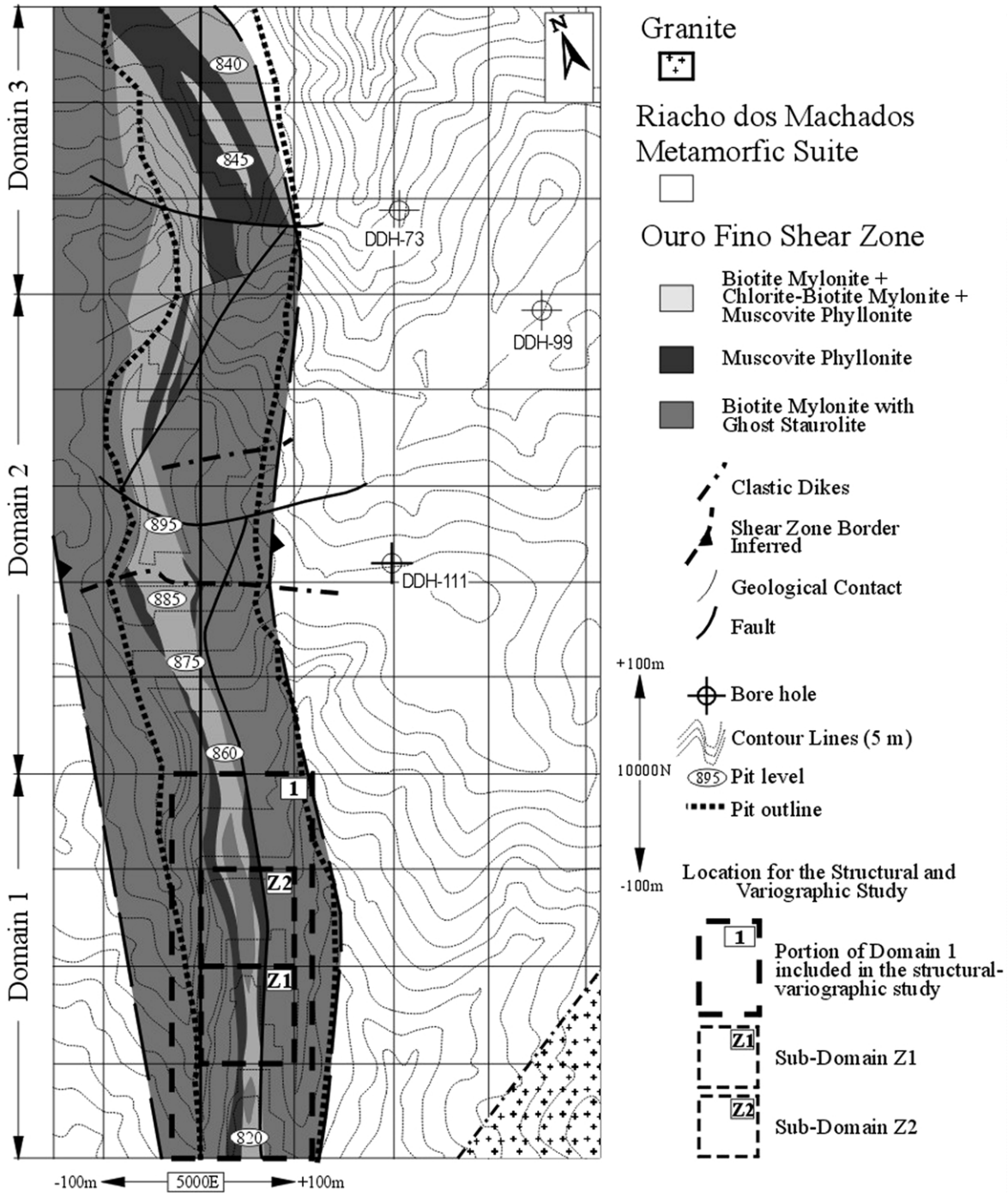

Fig. 4. Geologic map of Ouro Fino Mine (Monteiro, 1989; Docegeo, 1992; Monteiro, 1996). The granite, the Riacho dos Machados Metamorphic Suite, and the Ouro Fino Shear Zone are the three tectonic-stratigraphic units present near the mine pit. Domain 1 and its sub-domains Z1 and Z2 are the focus of the structural variographic analysis carried out in the present work.

stretching lineation (staurolite–ghost) within the shear zone characterized by pseudomorphic substitution by muscovite. This lineation is sub-parallel to the biotite mineral lineation.

There are three main tectonic–stratigraphic units in the vicinity of the mine (Fig. 4): (1) granite; (2) Riacho dos Machados Metamorphic Suite; and (3) shear zone rocks. Within the mine open pit, five different rock type groups were recognized based on composition, texture–structure and formation processes:

1. The regional metamorphic rock unit, represented by biotite schists and biotite gneiss, is part of the Riacho dos Machados Metamorphic Suite and includes rocks with an

iron-rich metapelitic derivative mineral assemblage metamorphosed at middle amphibolite facies (± kyanite, ± staurolite, ± garnet, biotite, plagioclase and quartz). Mesoscopic features include: (a) banding varying from 1 to 5 mm; (b) porphyroblastic staurolite, which is up to 1.5 × 6.0 cm; (c) porphyroblastic garnet, up to 4 mm in length; (d) mineral lineation, defined by biotite; (e) flattened staurolite; and (f) lepidoblastic texture. The prominent fabric is L–S, in which the biotite defines mineral lineation and foliation. The staurolite orientation is generally oblique to the mineral lineation, and is flattened with different degrees of transposition toward the mineral lineation. The rock color is medium to light gray, and light red when weathered. Some specimens show compositional layering, varying from 1 to 15 mm in thickness, which could represent an original depositional feature transposed by the regional event; some of these layers are rich in graphite. Within this rock type group the gold-hosting shear zone was established.

2. The shear zone-related metamorphic rocks, generally represented by biotite mylonite, are characterized by: ± garnet, ± plagioclase, quartz and biotite. Hand specimens of biotite mylonite show the following structures or textures: (a) granolepidoblastic fabric, with alternating felsic and mafic layers of about 1–2 mm; (b) biotite defining a mineral lineation; (c) staurolite with sericite–muscovite pseudomorphs, defining the stretching lineation, which is sub-parallel to the mineral lineation. The pseudomorphs are indicted by small circles of about 5 mm in diameter on sections parallel to *zy*; on sections parallel to *xz* these pseudomorphs are up to 8 cm. The rock color is medium to light gray or brown, and is light red when weathered. The altered biotite mylonites are also evident by a green–grayish color. When these altered rocks are weathered they lose their fabric, showing a massive aspect. In thin section, textures from pyrrhotite indicate syn-tectonic growth, whereas pyrite and arsenopyrite textures indicate late to post-tectonic growth. The arsenopyrite is euhedral and shows zoning of Co and Ni and normally replaces pyrrhotite, and sometimes pyrite.
3. The shear zone-related hydrothermal metamorphic rocks, generally referred to as muscovite phyllonite, are characterized by: ± garnet, ± plagioclase, ± tourmaline, muscovite and quartz; the enveloping alteration assemblage, which overprints biotite mylonites, is ± chlorite, ± sericite, ± tourmaline, ± carbonate. The muscovite phyllonite is always enveloped either by biotite mylonite or chlorite–sericite bearing biotite mylonite. Direct contact with the rocks of the metamorphic suite was not observed. Most commonly, the altered biotite mylonite envelops the muscovite phyllonite. On outcrop scale, phyllonite shows: (a) grano-lepidoblastic texture, with alternation of fine layers of muscovite and quartz; (b) mineral lineation defined by muscovite; and (c) numerous quartz-veinlets. The rock color is light gray and its grain size is usually smaller than 1 mm. When it is weathered, the rock is pale beige, friable and soft. In thin section, pyrrhotite shows syn-tectonic textures, and its shape is influenced by the mylonitic foliation. Chalcopyrite, pyrite and arsenopyrite replace pyrrhotite and usually form subhedral to euhedral crystals. The arsenopyrite shows zoning produced by variation in nickel concentration (Fig. 5B and C). The decrease of nickel content is normal toward the edge of the crystals, and the same applies to pyrite nickel contents. The chalcopyrite–pyrite–arsenopyrite association replaces early pyrrhotite and also fills open spaces produced during late movements of the shear zone (Fig. 5A). Gold is present in three main habitats: (a) filling fractures inside arsenopyrite, (b) blobs inside arsenopyrite, and (c) at the interface of arsenopyrite with the mylonitic foliation.
4. Quartz veins and aplites follow the host foliation and also cross-cut it. The contacts of quartz-veins and aplites sometimes have alteration selvages. The thickness of the selvages varies from a few millimeters up to 2 m in an extreme case, and the most important mineral phase is quartz. Aplite dykes are mostly composed of feldspar and quartz, showing a micro-granular texture that gives the rock a massive aspect. They are weathered, friable, white, and are usually discordant; however, sometimes they follow the foliation planes. The contacts produce a narrow alteration halo that is always weathered and difficult to sample. These veins and aplites are usually thinner than 15 cm.
5. Sub-vertical quartz sandstone dikes, with subarkose composition are generally referred to as clastic dikes; they cut the shear zone at 90°. A typical estimated modal composition of this clastic dike is 85% quartz, 15% K-feldspar, and has traces of lithic fragments, zircon and sericite.

Algebraic analyses of the composition and reaction space, including biotite gneisses, biotite mylonites and muscovite phyllonites, were carried out to determine the metamorphic sequence at Ouro Fino. This study showed that the mylonites were created at the expense of the surrounding gneisses, and finally, the mylonites were transformed into phyllonites during the hydrothermal metamorphism (Monteiro, 1996).

Gold is not particularly located in veins but it is mostly disseminated into the phyllonites. However, some economic grades are also found in the mylonites and their altered equivalents. Gold and arsenopyrite are closely associated (Fig. 4), and based on their textural and structural features, observed in thin section and microprobe analysis, the mineralization occurred late in the evolving shear zone system mostly using structural traps of various scales (Monteiro, 1996).

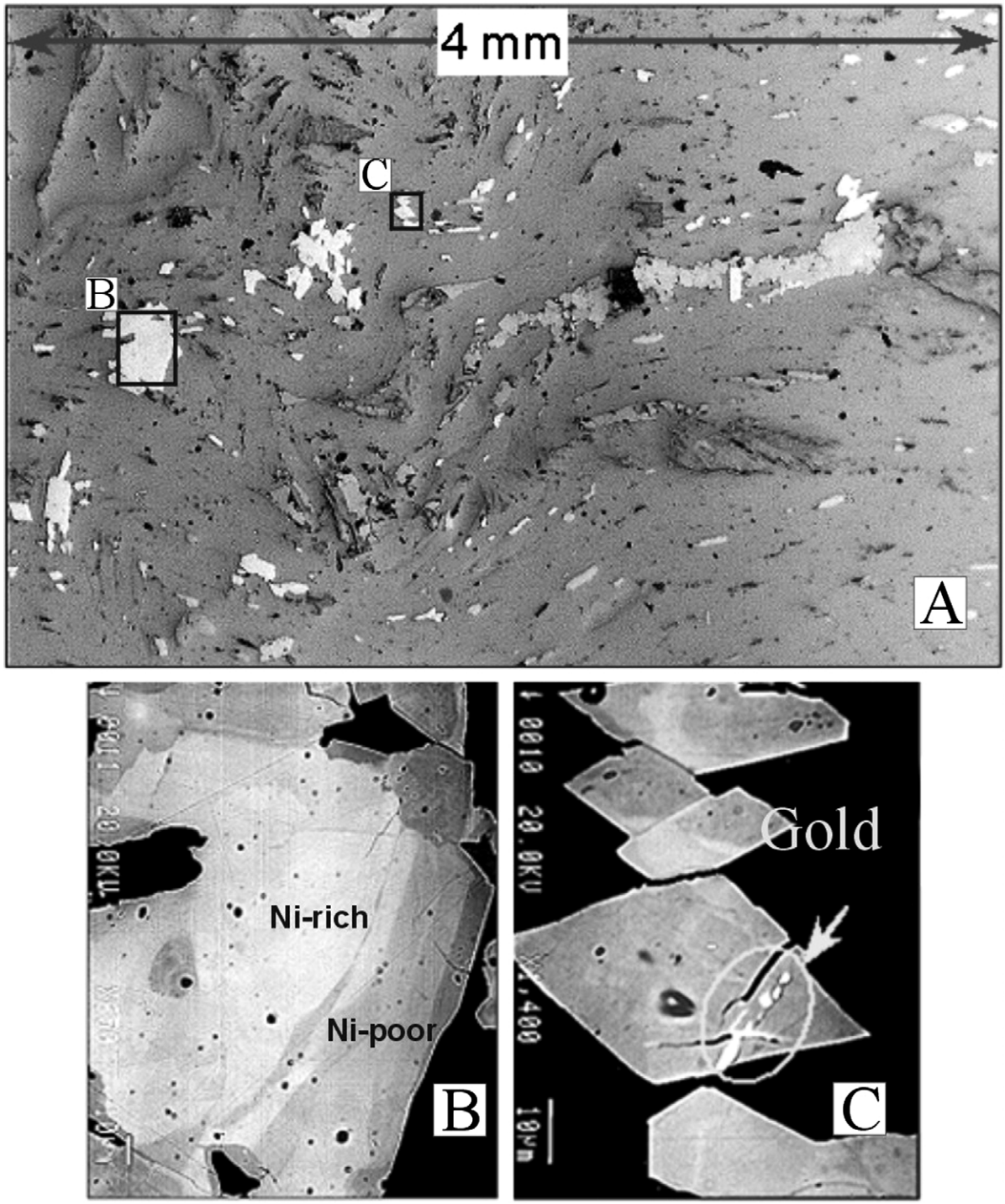

Fig. 5. The micro-crenulation presented in this figure is one of the features that controls gold distribution in the deposit as indicated by the structural analysis and structural variographic analysis (DDH-073-depth 94.00 m). (A) Micro-crenulation and clusters of arsenopyrite; under reflected light (viewpoint is orthogonal to the axis of crenulation). Note that the locations of (B) and (C) are indicated. (B) Arsenopyrite showing a complex zoning in nickel concentration (light gray represents Ni-rich zones, dark gray represents Ni-poor zones—backscatter image). (C) Clustered euhedral arsenopyrite grains; observe the small blobs of gold inside the arsenopyrite or filling micro-fractures (backscatter image).

3. Applied structural-geostatistics

Three distinct macro-domains were characterized in the mine (Fig. 4), in which geology, structural architecture and grade distribution show different configurations. Domain 1 is at the south end of the mine and it has two parallel bands of muscovite phyllonites, separated by a biotite mylonite unit. The ore bodies in this domain show lower grades when

compared with the other domains, but maintain a more regular distribution. Domain 2 is in the center and has irregular distribution of muscovite phyllonites; in this domain the gold grade is reported to be erratic. A thicker band of muscovite phyllonites striking north characterizes Domain 3 at the north end of the mine, where gold grades in the ore bodies are higher (Belo, 1994b). Details on further subdivisions will be discussed later.

3.1. Structure

The broad structural architecture of the mine is introduced in this section Our particular interest is to describe the possible small- and large-scale structural features that were available for the mineralized fluid to flow in. Features that are particular to each domain will also be introduced (see Fig. 4 for domain locations). Planar and linear structural features are described initially, followed by folds, their intersection lineations, and faults.

3.1.1. Planar elements

Three planar fabric elements were recognized within the mine open pit: S, C and C′ structures (Fig. 6; the surfaces are represented as vectors—dip-direction/dip—and not as poles, and the isolines follow this representation). These form the S–C and C–C′ pairs as described in Berthé et al. (1979) and Lister and Snoke (1984). The S–C pair overprints the regional foliation (Sn) that is characteristic of the biotite gneisses. Within the shear zone, recognition of this earlier surface is facilitated when well-developed mica-rich staurolite-pseudomorph relicts are present in the rock. The S–C pair is the prominent mesoscopic structure found in the biotite mylonites. It can be further described as type II S–C mylonite (Lister and Snoke, 1984). However, in the muscovite phyllonites, only the C surfaces are well-defined in hand specimens because of the higher deformation, coupled with intense recrystallization and neoformation. At this scale, it is difficult to compare the timing of the formation of the S–C pairs between biotite mylonites and muscovite phyllonites. However, thin section observations indicated that the phyllonitization process overprinted the mylonites. In addition, metamorphic studies on mineral assemblages, in their composition and reaction space, have confirmed the same sequence of events (Monteiro, 1996). The S surface maximum concentration (151°/50°, dip-direction/dip) and the C surface average plane show a northward migration from south to north, indicating a counter-clockwise rotation—119°/50°, 112°/46° and 082°/50° in Domains 1, 2 and 3, respectively (Fig. 6). The S–C pair intersects at 45° towards 143°. The C–C′ pair, which is represented by an incipient muscovite–chlorite foliation overprinting the S–C pair, is better identified within Domain 3. Quartz veinlet surfaces generally follow the C surface (Figs. 6 and 12).

3.1.2. Linear elements

The stretching lineation (ls) is defined by ghost staurolite crystals that can be up to 8 cm in size This structure is only observed within the biotite mylonites and it is usually sub-parallel to the mineral lineation. It has two main concentrations: one at 45°/146° (plunge/trend) and the other at 45°/123° (Fig. 7). In shear zones where the bulk symmetry of the internal structures is near monoclinic, the stretching lineation should plot perpendicular to the intersection of the S–C pair; however, natural processes can promote diverse shear zone configurations (Lin and Williams, 1992), and later translation–rotation in an evolving shear zone could have caused migration of the S–C pair. In the case of Ouro Fino Mine, the stretching lineation plots near the intersection of the S–C pair, suggesting rotation of S along the C surface. In addition, the 55–78° rake of the stretching lineation over the C surface indicates that the shear zone was developed over an oblique ramp.

On the C surfaces, the development of a mineral lineation, determined by the phyllosilicates, is characteristic (38°/135°). However, on the stereonet this mineral lineation shows a girdle, which also follows the average C plane, suggesting a complex behavior along the shear zone. In Domain 1, this mineral lineation shows uniaxial symmetry, with a maximum at 37°/149° (Fig. 7).

3.1.3. Folds

Folds range from crenulations up to outcrop-size. Crenulations observed throughout the Ouro Fino Mine are considered to be third-order parasitic folds with wavelengths normally around 5–20 mm and related to the first-order larger folds. These third-order plunging asymmetric folds are normally open with well-defined curved hinges. Three main intersection lineation styles related to the third-order folds were recorded and their average spatial orientations are li(1), 39°/139°; li(2), 39°/124° (less evident); and li(3), 10°/195°–02°/030°. Stereonet plots for these intersection lineations, presented by type and by domain, are shown in Fig. 8. The stereonet plot, which includes all intersection lineations, shows a girdle that mimics the spatial orientation of the average C surface. The overall vergence presented by these crenulation sets is left-lateral and reverse, towards the São Francisco Craton. Field observations indicate that these sets cross-cut each other, suggesting contemporaneous development. Nevertheless, the rotation of li(3) toward li(1) was observed during field work. The average angle, measured in hand specimens, between li(1) and li(3) is 48° (44 counts, ± 15°) ranging between 16 and 80°. High variability was observed transversal to the shear zone strike. As indicated before, gold-hosting arsenopyrites also cluster along the crenulation axes (Fig. 5A), suggesting that these structures are significant controllers to the mineralization, as will be shown.

The second-order parasitic folds share the same

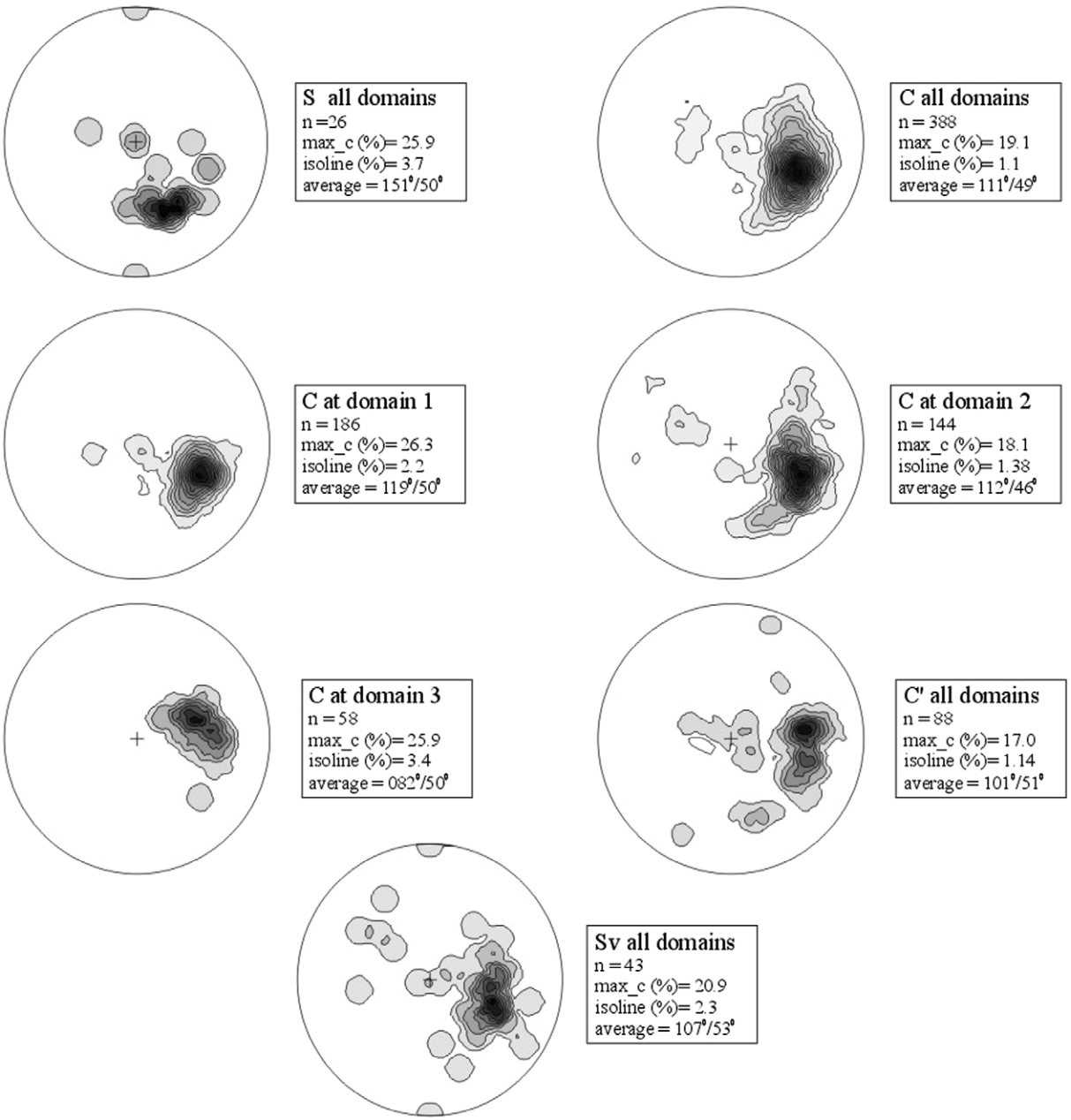

Fig. 6. Stereonets of planar fabric elements observed in the Ouro Fino Mine pit. The C surface is also presented for each domain (see Fig. 4 for domain location). Note that the isolines in these stereonets are representing the vector dip-direction and dip of the structures and not their poles.

characteristics observed for the crenulations, however, their wavelengths vary from 15 to 30 cm. These folds are rarely observed within the open pit. One unusual fold of this group was observed on level 885-S within Domain 2 (Fig. 9A and B). This fold has its hinge sub-parallel to the mineral lineation, which is also sub-parallel to the local vergence vector. The hinge is curved with a spatial orientation varying from 115 to 136° in trend and from 30 to 45° in plunge. A mineral lineation is less than 15° to this fold axis. First-order folds are observed in very few places, and the best example is at the 890-S open pit level (Domain 2; Fig. 9C). This fold is similar to the third- and second-order fold sets, except for its wavelength, which is around 5 m. The second- and first-order folds presented in Fig. 9 are comparable with the crenulation orientations of li(1) and li(3), respectively.

3.1.4. Other structures

Evidence for a late eastward backward movement is noted where the tips of some meso-scale faults are rotated toward the east. In addition, the tips of vertical quartz-filled tension gashes indicate the same displacement sense. Clastic dikes that are present on the mine pit are believed to represent the infilling of open fractures in the basement by the cover sequence (Belo, 1994b), These type of dikes are commonly associated with fold-and-thrust belts worldwide

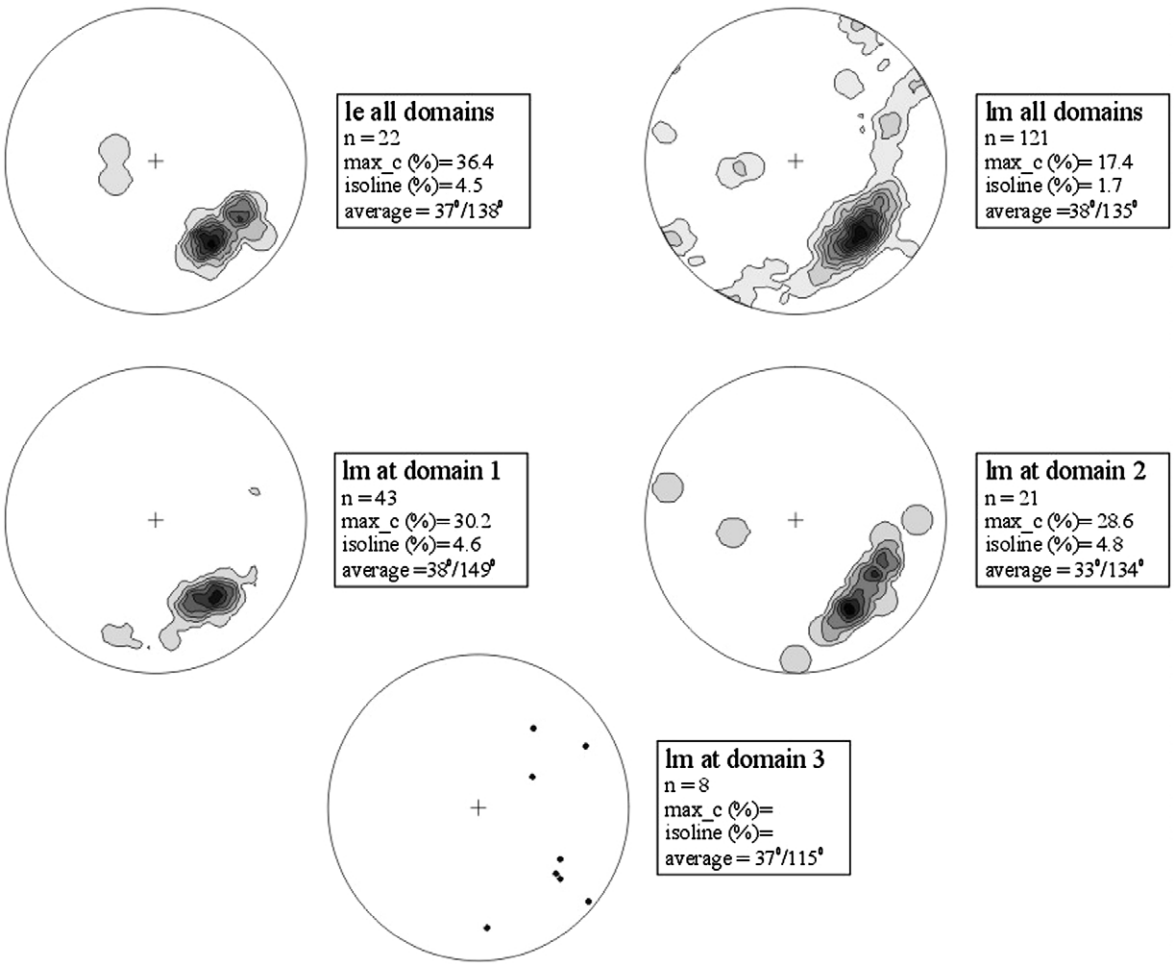

Fig. 7. Stereonets for stretching lineations (ls) and mineral lineations (lm). Mineral lineations are further sub-divided into domains (see Fig. 4 for domain location).

(Powell, 1969; Brock and Engelder, 1977; Winslow, 1983; Barber et al., 1986). A paper describing in detail these clastic dikes, including implications for the shear zone evolution is in preparation.

Structural features and kinematic indicators observed in the mine pit (S–C and C–C′ spatial relations, mineral lineation, stretching lineation, and asymmetric crenulation) provided us with an estimated vector of tectonic transport for shear zone, which falls within the 300–325° trend.

3.1.5. Structural evolution

The Ouro Fino Mine shows a complex configuration of geological structures that were created and modified during subsequent phases The regional fabric is highly transposed within the shear zone and a new fabric represented by the S–C pair is registered in the mylonitic rocks. However, the S–C pair is progressively rotated and translated counter-clockwise during each reactivation pulse.

Asymmetric crenulations, pervasive throughout the pit, are useful kinematic indicators within the shear zone. The cross-cutting relationship of these folds, as well as the variation of the angles among them, suggests that they were progressively rotated. It seems reasonable to infer that the main movement inside the shear zone was a combination of two different components. One component was probably westward, while the other was northward. Considering the mutual interference of the resulting fabric elements, they were probably the result of recurrent episodes of deformation. The outline and relationship of fabric elements presented in this study suggest that the Ouro Fino Mine was developed over a slightly oblique ramp, which is in agreement with the orientation of the fold patterns observed in the mine.

The vector of tectonic transport estimated at the mine is towards 300–325°, which is in agreement with that defined for the cover fold-and-thrust belt as indicated previously, suggesting that the fabric elements overprinting biotite mylonites may have been produced during the Brasiliano reactivation of the basement shear zones.

3.2. Geostatistics

Geostatistics is concerned with the spatial distribution of

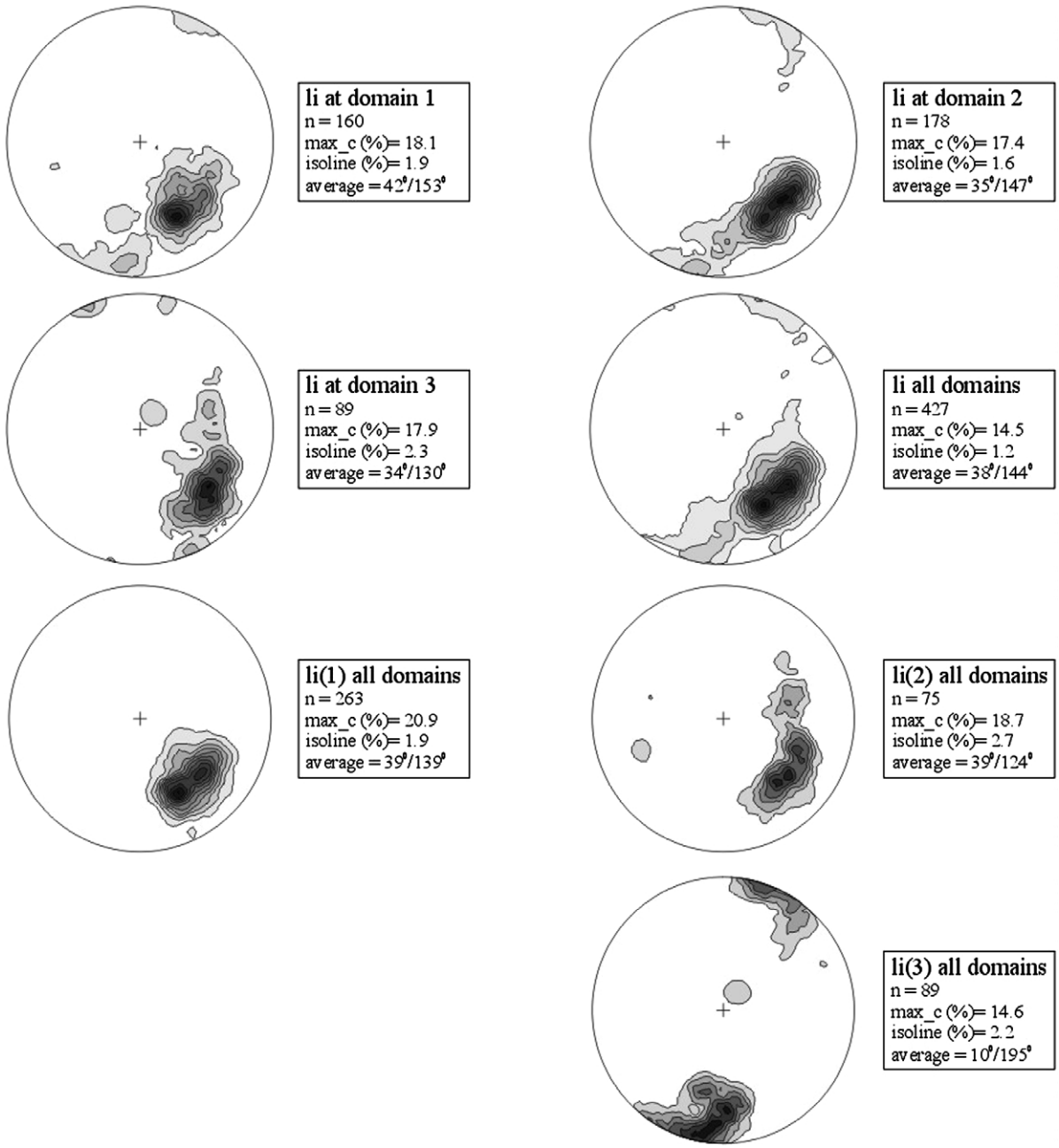

Fig. 8. Stereonets for intersection lineations (li) by domains and by types (li(n), where n is 1, 2 or 3). See Fig. 4 for domain location.

values, and was originally developed for the purpose of ore deposit modeling and ore reserve estimation (Matheron, 1963) However, the main goal behind the work of an ore deposit structural analyst is to understand the behavior of grade distribution and to correlate this information with the structural features of the deposit. The cornerstone of geostatistics is the semivariogram function, or the variogram as it is generally referred to by geostatisticians (Fig. 7). Given two locations, x and $(x + h)$, a variogram is a measure of one half the mean square error produced by assigning the value $z(x + h)$ to the value $z(x)$ (Olea et al., 1991), or the variance of the increment (Journel and Huijbregts, 1978). The variogram function is expressed by the following equation:

$$\gamma(h) = \frac{1}{2N(h)} \sum [z(xi) - z(xi + h)]^2 \quad (1)$$

where $N(h)$ is the number of experimental pairs $[z(xi), z(xi + h)]$ of data, separated by the vector h. The main structural features related to a variogram function are presented in Fig. 7. To assign a physical and geological meaning, the acquired experimental variograms (David, 1977) need to be fitted to theoretical variograms. There are many types of theoretical variogram models indicated in the

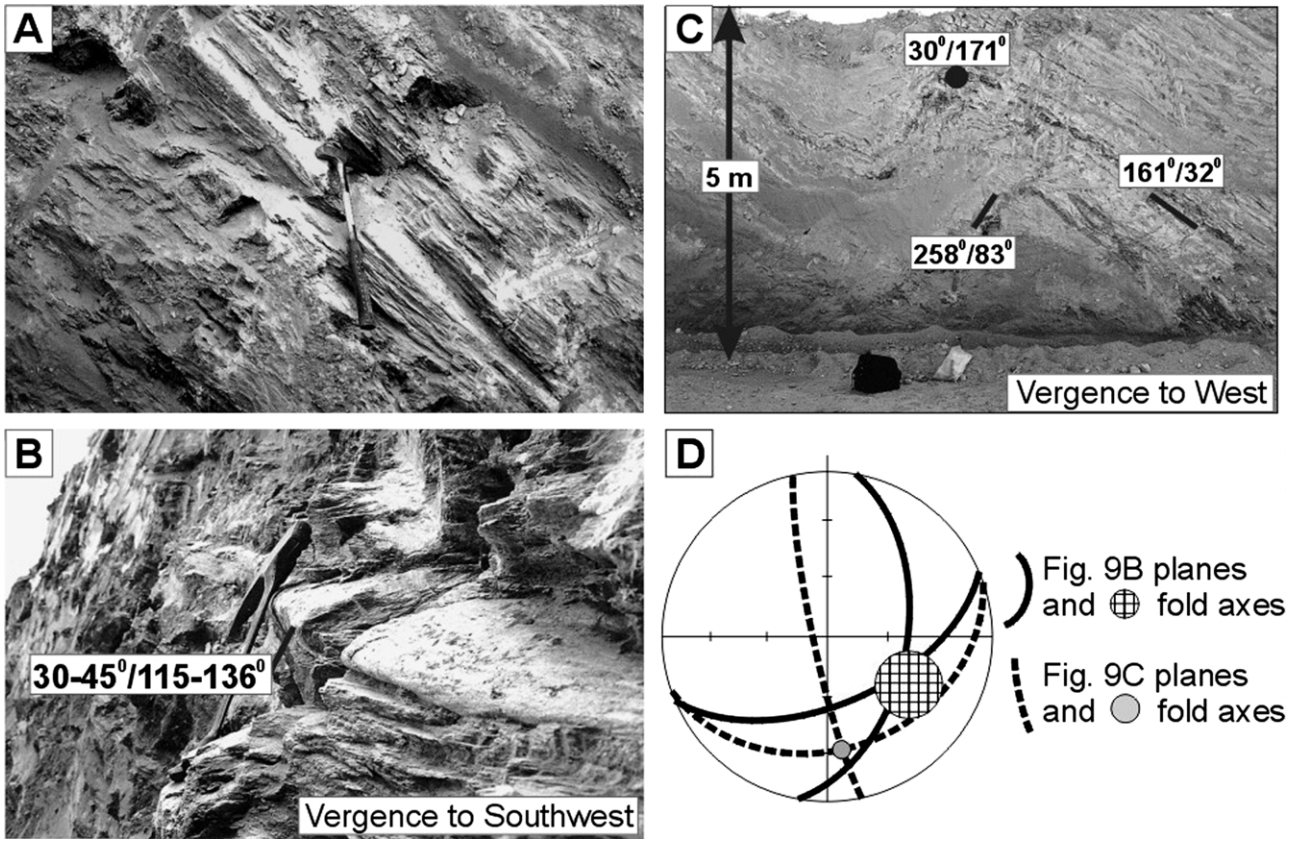

Fig. 9. Example of folds of different scales present on the pit. (A) Frontal view looking towards north of the grid. (B) Low angle oblique view, a second-order parasitic intrafolial fold with curved axis (30–45° towards 115–136°) is shown. The upper limb of this fold is 157°/56° and the lower limb is 100°/50°. Two mineral lineations were observed: 20°/090° and 12°/229°. The vergence of this fold is to the southwest (south side of the 885-S pit level, Domain 2). (C) A first-order plunging asymmetric fold observed on the 890-S pit level. The upper limb is 161°/32° and the lower limb is 258°/83°; the axis is 30°/171°. Two sets of intersection lineations were observed in this outcrop: 26°/173° and 46°/144°. The vergence of this fold is to the west (Domain 2). (D) A synoptical stereonet showing the fold limbs and fold axes ((B) and (C)) is presented.

literature (Olea et al., 1991); in the current work the spherical model was used (Matheron, 1963). The mathematical expression for the spherical model is:

$$\gamma(h) = C^{*}\left[\frac{3}{2}\left(\frac{h}{a}\right) - \frac{1}{2}\left(\frac{h}{a}\right)^{3}\right]; \qquad \text{if } 0 \le h < a \tag{2}$$

$$\gamma(h) = C; \qquad \text{if } a \le h \tag{3}$$

where C is the sill, and a is the range. If a nugget effect (David, 1977) is evident, it has to be added to the model.

3.2.1. Mineralization and anisotropy

The directional dependence phenomenon rendered by an economic element in a mineral deposit is defined as anisotropy (Journel and Huijbregts, 1978), and this is a fundamental feature in geostatistics, since grade is space dependent. Hence, the structural evaluation of grade distribution must include the study of anisotropy and its various degrees and shapes. Directional variograms are the tools to perform this study; the process of modeling these diagrams is called structural analysis in the context of geostatistics (Journel and Huijbregts, 1978); however, to avoid misinterpretation we will refer to it in the present work as *structural variographic analysis*.

In the interpretation and modeling of variograms, the range value and its variation must be carefully evaluated in different directions. The determination of the mineralization spread represents the backbone of structural variographic analysis. The next step is to define the shape and orientation of the mineralization anisotropy. Perfectly isotropic mineralization phenomenon should produce identical variograms in all directions. Conversely, anisotropism 'deforms' the isotropic sphere along the preferred direction of maximum similarity, creating an ellipsoid.

Several methods are found in the literature to best fit an ellipse or an ellipsoid to a dataset (Milton, 1980; Gendswill and Stauffer, 1981). The method used in the present work is from Matsumura (1981), which extracts the eigenvectors and eigenvalues of the covariance matrix from the range values or vectors determined during variogram modeling. Range vectors should plot at or near the surface defined by the best-fit ellipsoid, and the degree of anisotropy is the ratio between the largest and the smallest eigenvalues. The orientation of maximum range values is intuitively the

vector of mineralization, which characterizes a *geostatistical fabric element* (Monteiro, 1996). However, the interference pattern of nested structures, the directional characteristics of nugget and hole effects, is also part of the geostatistical fabric of a given mineral deposit. For instance, the directional dependency of hole effects (Journel and Huijbregts, 1978) can indicate the periodicity of ore shoots and low-grade zones. Recurrence of ore shoots is another important geostatistical fabric element, which has length and direction, and the inherent ability to predict hidden ore shoots.

3.2.2. Applied variography

A total of 37,673 samples were available for this study and the vast majority of them were sequential samples with approximately constant volume and shape (1.0 m × 0.15 m × 0.10 m), taken in regularly spaced lines that cut through the open pit section; some samples are from boreholes The average horizontal distance between lines was 13 m (± 2.5 m). Mine benches were made at 5 m intervals. The whole database, representing all domains, enclosed a volume of approximately 1200 m to the north, 200 m to the east and 100 m in depth.

Although we have run general statistics and variograms on the whole dataset, we focused our structural geostatistical analysis only on Domain 1, which represents a volume of 400 m to the north, 150 m to the east and 100 m in depth, where 11,727 samples were available. However, domains Z1 and Z2 are the center of our 3D structural geostatistical analysis. The dimensions of these two domains are approximately 200 m to the north, 100 m to the east and 100 m in depth, where 5728 samples were available, from which 881 were from boreholes. These two datasets were compared using the *t*- and *f*-tests (Hassard, 1991; StatSoft, 1998). Based on our calculated *t* value of 0.162 and calculated *f* values of 0.228 (two-tail test), 0.885 (one-tail test—upper), and 0.114 (one-tail test—lower), we concluded that at 95% confidence level there was no genuine difference between their means and variances.

The database provided by the mine technical staff was multiplied by a constant value to maintain the mining company's confidentiality. This technique does not change the sample variance–range vector relationship and it still allows variographic structural analysis, since the aim is to partition the a priori variance and extract the range vectors to determine the anisotropy of the mineralization (Monteiro, 1993, 1996).

Initially, summary statistics and frequency distribution plots were calculated using the moving-window technique to characterize the sample distribution and its general features through the deposit. This procedure indicated that the sample distribution closely follows the lognormal distribution. Therefore, a lognormal transformation was applied to the dataset to avoid undesirable variations on the sill of the variograms (Fig. 10). After these initial transformations, directional variography of log-transformed values was carried out within contained structural domains previously defined by structural analysis.

A critical component of ore deposit structural analysis is to confine directional variography within the domains dictated by the fabric elements, which is the only methodological bridge that brings structural geology and geostatistics together, allowing further intrinsic comparisons. At Ouro Fino Mine, Domain 1 was selected for structural–geostatistical examination because of its simpler configuration of the fabric elements when compared with the other two domains. Within Domain 1, two sub-domains (III-Z2 and III-Z1; Fig. 4) were further defined, based on structural geology, rock and sample distribution features.

Several tests were conducted to define the parameters to calculate stable 3D variograms, including sample line spacing and sample density on each variographic direction, and varying the set of parameters in different directions to evaluate variogram stability. Several variographic directions (000°, 020°, 040°, 060°, 080°, 090°, 100°, 120°, 140° and 160°) were tested, with different dip angles (00°, 15°, 30°, 45°, 60°, 75° and 90°). As a result, the directional dependency of the range value (range vector) obtained during the modeling was used to evaluate the shape of the ellipsoids that best described the structures observed during the structural analyses. An example of variograms obtained for Ouro Fino is presented in Fig. 11.

Two nested variograms, as described in Journel and Huijbregts (1978), were identified during variogram modeling, which suggest the existence of two grade distribution patterns at two different scales (Fig. 11). The small range vectors (C(1)) and the sub-domain scale large range vectors (C(sill)) were used to build a covariance matrix for each structure, and the eigenvalues with associated eigenvectors were calculated. The results of this work are presented in Table 1.

The different ellipsoid parameters and their aspect ratios were plotted on a modified version of the Flinn diagram (Ramsay and Huber, 1983) to demonstrate the shape and degree of anisotropy of the small and large range mineralization ellipsoids (Fig. 12B). The small range ellipsoids from Z1 and Z2 sub-domains yielded very different results, plotting in the triaxial and oblate fields, respectively. However, the large range ellipsoids yielded similar aspect ratios from the same sub-domains, and more interestingly, their shape is intermediate to the extreme cases defined by the small range ellipsoids.

3.3. Structural geology and structural geostatistics connections

Upon determining the spatial orientation and scale of existing fabric elements, synoptical stereonets are produced to establish the common ground between the traditional structural and variographic analyses, provided they were obtained within the same structural domain Fig. 12 introduces two stereonets, one for each sub-domain (Z1 and Z2),

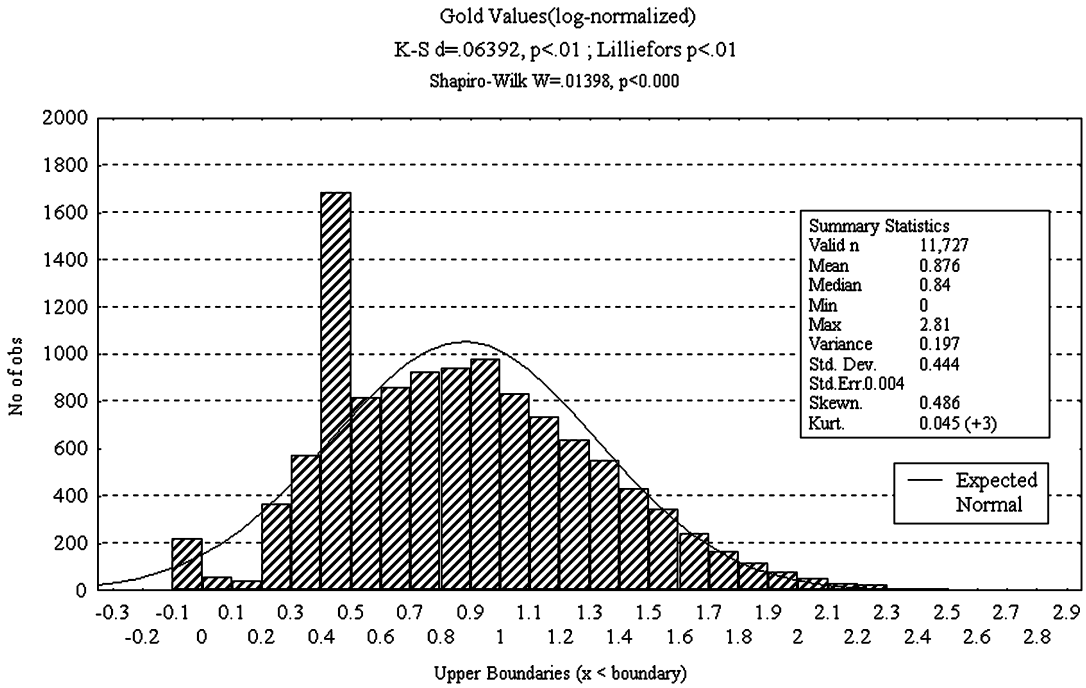

Fig. 10. Distribution frequency of gold values for samples located in Domain 1 (logarithm of the values).

in which the three vectors (major, intermediate, and minor) that define the small and large range ellipsoids (Table 1) are indicated. The similarity of mineralization axes or vectors and structural elements is remarkable. The most prominent feature is that the major and intermediate mineralization vectors of both the small and large range vectors plot near or at the C surface.

In sub-domain Z1, both small and large range major mineralization vectors plot near the sub-horizontal intersection lineation (li(3)), and along the direction of the C surface. Both the small and large range intermediate mineralization vectors plot near a cluster of fabric elements: stretching lineation, mineral lineation, and the other sets of intersection lineations (li(1) and li(2)). As a result, the minor mineralization vectors are close to the pole of the C surface. The small range ellipsoid is triaxial and conformable with the sub-horizontal fabric that represents the micro-, meso- and macro-scale asymmetric folds.

In sub-domain Z2, the same general pattern was observed; however, both the small and large range major mineralization vectors plot near the prominent cluster of fabric elements, while the small and large range intermediate mineralization vectors tend to plot near the shallower dipping folds and crenulations (li(3)). As expected, the minor mineralization vector is close to the pole of the cluster of fabric elements. Both small and large range ellipsoids are oblate in this case and conformably close to the C surface as well.

These results suggest that the evolution of the mineralization was closely related to the evolution of the rock fabric. Particularly, the C plane spatial orientation seems to have been the main percolation duct, in which the mineral and the stretching lineation orientations, along with the intersection lineation (li(1) and li(2)), greatly facilitated the fluid flow along the shear zone surfaces. The striking coincidence of sub-horizontal intersection lineation (li(3))

Table 1
Eigenvalues (E_1, E_2, and E_3) and respective eigenvectors (t_n = trend, and p_n = plunge; where n is 1, 2 or 3). The ratio between major and intermediate axes (e_1/e_2) and intermediate and minor axis (e_2/e_3) is shown. The small range vectors are represented by C(1), while the large range vectors are represented by C(sill). The ratio e_1/e_2 for C(1) and C(sill) from Domain 1 are apparent ratios, since the variograms were only horizontal

	E_1	E_2	E_3	t_1	p_1	t_2	p_2	t_3	p_3	e_1/e_2	e_2/e_3
III C(1)	27.9	9.4	0.0	25	0	295	0	0	0	2.97	–
III (sill)	93.2	36.2	0.0	22	0	292	0	0	0	2.57	–
Z1 C(1)	54.9	35.9	23.9	29	9	136	60	294	28	1.53	1.50
Z1 C(sill)	106.3	73.3	43.2	34	11	134	41	292	47	1.45	1.70
Z2 C(1)	43.6	41	21	171	29	54	40	286	37	1.06	1.95
Z2 C(sill)	127	109.6	69.9	113	67	12	5	280	22	1.16	1.57

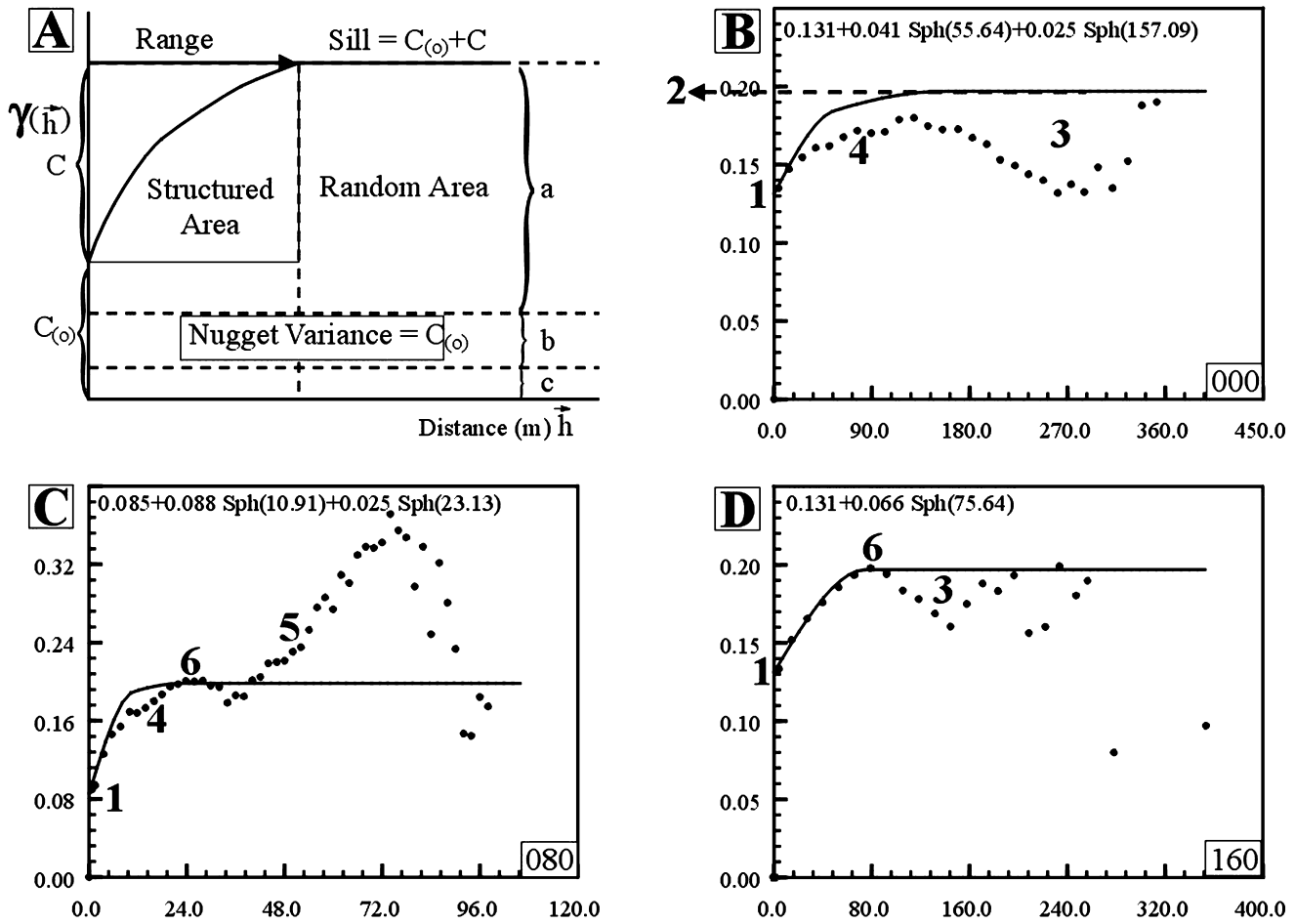

Fig. 11. Characteristic variogram profiles for Domain 1. (A) A typical spheric model variogram is shown. The vertical axis is the variance of the population partitioned in two sectors: C(0), or the nugget effect, and C, the part of the variance that explains the structured area. The small *a* represents the part of the variance that is natural to the deposit, and *b* and *c* represent sampling and analytical errors. A component of the nugget effect is related to natural features expressed in a smaller scale that is explored by the experimental variogram. The horizontal axis is the sample distance. The term *range* symbolizes the traditional concept of *zone of influence* of a sample, and it represents the distance where the variogram function reaches the sill (Matheron, 1963). The *sill* is the a priori variance of a random function, or simply the variance of the population. (B)– (D) experimental (dots) and theoretical (line) variograms for the directions 000°, 080° and 160° are presented, respectively, obtained in the current study to show some key features found in Ouro Fino Domain 1: (1) C(0) or the nugget effect, (2) C(sill) set at the a priori variance level, (3) hole effect when after the sill there are samples with higher autocorrelation, (4) small range vector, (5) drift of the function, and (6) large range vector when the experimental variogram reaches the sill.

with the major mineralization axis of Z1, as well as with the intermediate mineralization axis of Z2, indicates that this rock fabric played an important role in the final mineralization trapping. The mine geologists did not recognize this feature as an important control to the mineralization. The stretching lineation was the most followed feature during exploration and mining operations. The linkage between mineralization vectors and fabric elements provided us with a better understanding of the mineralization and its local deviations. Hence, mine geologists could recognize subtle variations in grade distribution direction just by visually inspecting the shape and orientation of key structures at the mine pit.

Another key aspect is the convergence of the small and large range ellipsoid shapes, in which the triaxial (Z1c1) and the highly oblate (Z2c1) small range ellipsoids evolved towards the intermediate oblate large range ellipsoids, suggesting that the operating fine-scale percolation fabric during the mineralization event was different in the two sub-domains, whereas at the integrated Z1–Z2 sub-domain scale the percolation fabric shared more structural and variographic similarities (Fig. 12B). In addition, 3D iso-surfaces of gold grades, produced using ordinary kriging (Matheron, 1963), are very helpful in indicating the general shape of the grade distribution on the selected domains (Fig. 13); in this figure the small and large range best-fit ellipsoids were also plotted for comparison.

Other studies that have attempted an integrated structural and variographic analysis of mineral deposits have produced comparable results, such as the one carried out on the Santa-Craze gold deposit in Western Australia (Newton et al., 1997; Newton, 2000). Other techniques also are being introduced in the field, such as Patterson–Leymarie–Fry analysis (Leymarie, 1968; Allison et al., 1997; Vearncombe

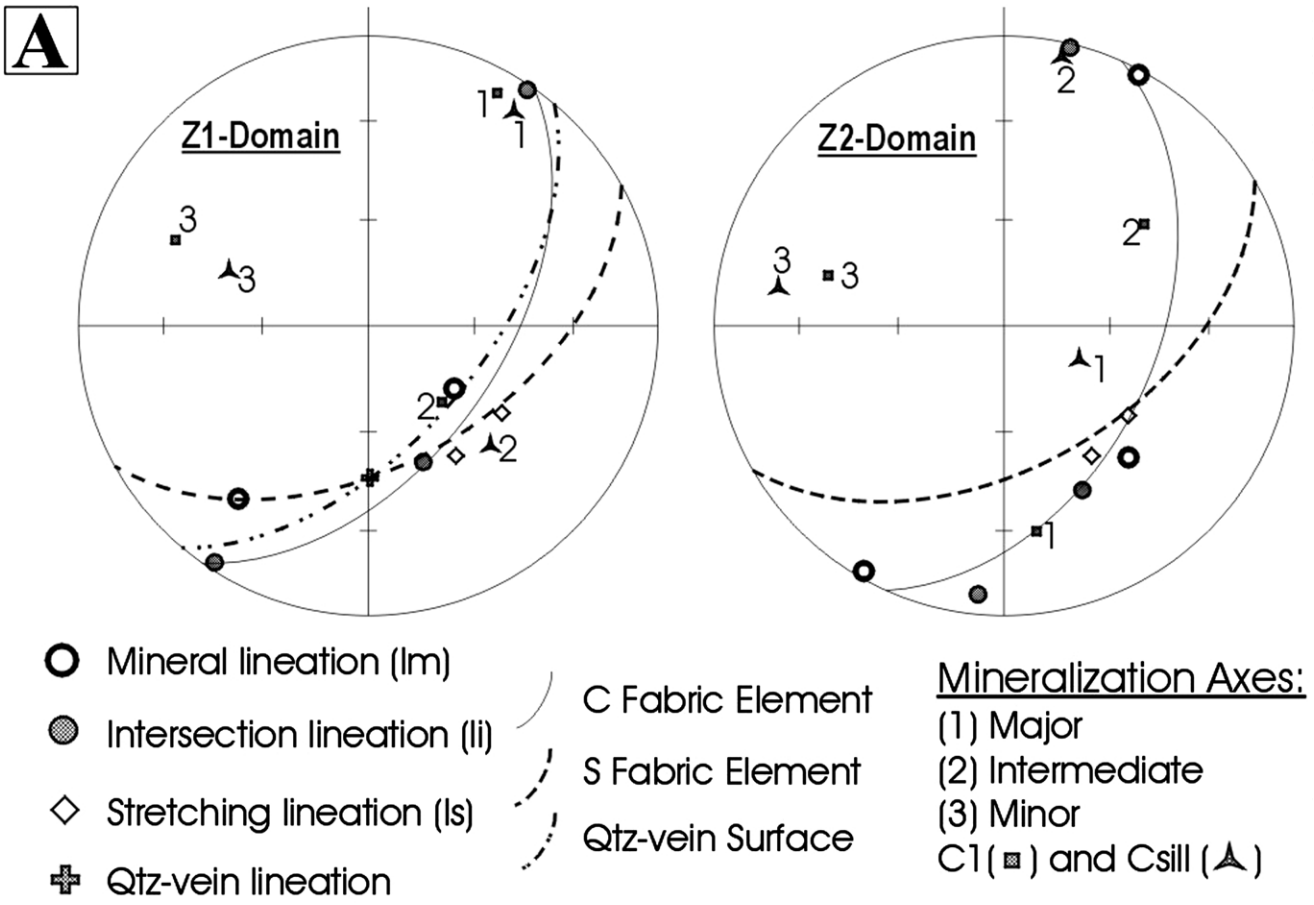

Fig. 12. Proposed linkage between structural and geostatistical elements. (A) Synoptic stereonets for sub-domains Z1 and Z2 (see Fig. 4 for location). At Z1: C (125°/52°), li (48°/158°–02°/034°–03°/213°), lm (60°/126°–26°/217°); S (all domains 151°/50°), and ls (all domains 45°/146°–45°/123°). At Z2: C (114°/46°), li (37°/154°–02°/013°–08°/186°), lm (38°/137°–02°/028°–02°/209°), S (all domains 151°/50°), and ls (all domains 45°/146°–45°/123°). The spatial orientations for the ellipsoid parameters are indicated in Table 1. (B) The mineralization ellipsoid to the left and the Flinn diagram to the right with the parameters of the mineralization ellipsoids plotted (adapted from from Ramsay and Huber (1983)) is presented. Note that the small range ellipsoids have strikingly different shapes while the large range ellipsoids are similar, indicating a shape convergence towards the integration of Z1 and Z2—that is, towards the scale of Domain 1.

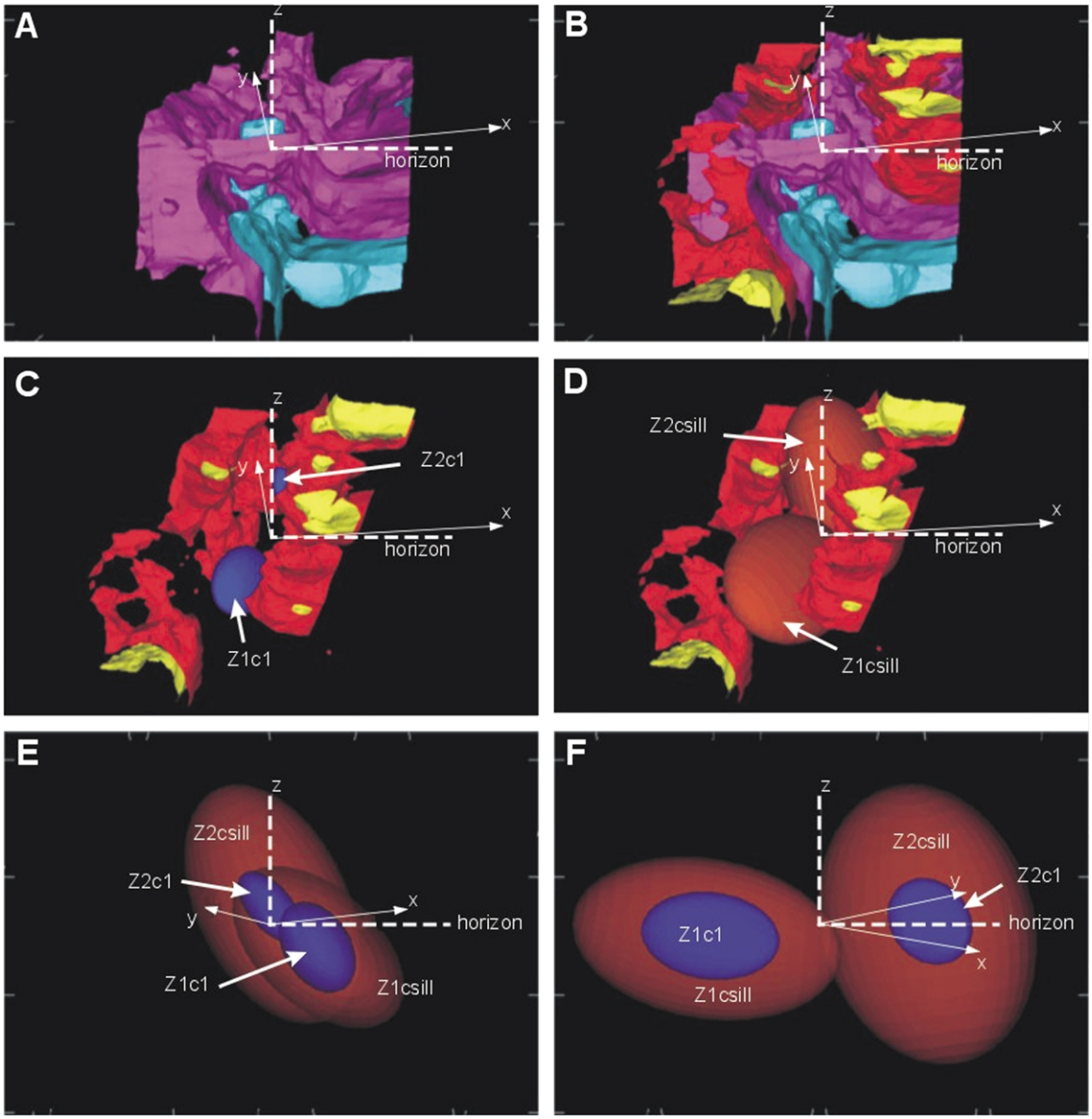

Fig. 13. 3D iso-surfaces representing four different log-transformed gold grades on domains Z1 (south) and Z2 (north) (blue = 0.34, purple = 0.86, red = 1.38, and yellow = 1.89). (A) Observe the 'folded' aspect of the blue and purple surfaces, including some holes along the central area (viewpoint at 20°/015°). (B) The surfaces representing the higher gold values (red and yellow) tend to form horizontal pipes. (C) Red and yellow iso-surfaces and the small range ellipsoids from domains Z1 and Z2 in dark blue (viewpoint at 34°/005°). (D) Red and yellow iso-surfaces and the large range ellipsoids from domains Z1 and Z2 in dark brown (viewpoint at 34°/005°). (E) Small and large range ellipsoids (viewpoint at 11°/034°). (F) Small and large range ellipsoids (viewpoint at 10°/315°). See Fig. 4 for domain location.

and Vearncombe, 1999) and Fractal analysis (Mandelbrot, 1982; Carlson, 1991; Costa, 1997). Recently, Blenkinsop (2002) evaluated the extrinsic features of orebodies from the Acturus and Shamva gold deposits (Harare greenstone belt, Zimbabwe) using best-fit ellipsoids to the ore shape produced by mineral resource analysis, with further successful comparison with the existing structural fabric.

4. Conclusions

This paper has described the various structural features present in the Ouro Fino Gold Mine open pit. Domain analysis, in which structural and geostatistical fabric elements were considered together, was used to demonstrate the linkage between structural geology and geostatistics, revealing their intrinsic association. At Ouro Fino Mine, ore deposit structural analysis has indicated that gold solutions followed two main clusters of rock fabrics. The main mineralizing fluid inflow was possibly upward along the thrust movement direction with lateral escape along the interconnecting sub-horizontal fabric. The results of these combined analyses have demonstrated the reliability of the grade-structure relationship and its estimation.

As suggested in this paper, the main goal of an ore deposit structural analysis is to arrive at an understanding not only about the extrinsic features, but also and more importantly about the intrinsic structural features that have controlled the formation and evolution of a mineral deposit. The immediate consequences of this work provide guidance to grade control and pit optimization during mining since the structural features that control grade distribution, determined during the ore deposit structural analysis, are noticeable on the mine pit.

Ore deposit structural analysis, as a combination of current structural geology and geostatistical tools, provided they are carried out within the same structural domain, is a powerful tool at the hands of a mine geologist during the development of the mine. Furthermore, this style of analysis helps in the design of more effective exploration strategies for the surrounding areas; combining traditional structural analysis with geostatistics into a new field that is currently taking shape. Structure, grade and shape are linked to the petrofabric and the realization that it can be measured using various combinations of tools and procedures has a crucial impact in mineral deposit evaluation and exploration, opening a tremendous field of opportunities for structural–economic geologists worldwide.

Acknowledgements

The contents and presentation of this paper have been improved as a result of the advice and contributions from several Inco Limited colleagues, in particular, Peter Lightfoot, Robert Grant, Olivier Tavchandjian, James Koronovich, Carl Laamanen, Dave Burrows, Robert Horn and Danielle Leger. Dominique Francois-Bongarcon and José L. Andriotti also reviewed the geostatistical aspects of this work. A Ph.D. grant from the Brazilian Council of Research (CNPq) funded this work, including a Teaching Assistantship from the University of Western Ontario granted to the first author, as well as by the Companhia do Vale do Rio Doce (CVRD–Docegeo). Docegeo's geologists Otoniel, Roney, Roberio and Tadeu are also thanked for their help. Jinchi Chu allowed the use of his Xgam variogram modeling software, and Sony Winardhy assisted with the program to estimate best-fit ellipsoids. Sahadia Koop, Leo Hartman, Alexis R. Nummer, Dagoberto Assis, Jair Koppe, João F.C. Leite, Juarez Fontana, Elisabeth Fonseca, Eric Schimidt, Robert Hodder, Norman Duke, Mike Powell, Robert Barnett, Keith Barron, Hamid Mumin and Kim Law helped in several aspects during the development and conclusion of the original work at Western. We also would like to thank Dr Tom Blenkinsop, Dr Stephen Peters and the anonymous reviewer from the Journal of Structural Geology for their valuable comments. We are grateful for the help and enthusiastic support directed from these colleagues and agencies.

References

Allison, I., De Paor, D.G., Haszeldine, R.S., Bowman, A., Maguire, M., 1997. Cryptic Structural Trends in Basement Revealed by Patterson Diagrams: Examples from the Scottish and Irish Caledonian orogen, Chapman & Hall, London, pp. 487–495.

Almeida, F.F.M., 1977. O Cráton do Sao Francisco. Revista Brasileira de Geoscências 7, 349–364.

Barber, A.J., Tjokrosapoetro, S., Charlton, T.R., 1986. Mud volcanoes, shale diapirs, wrench faults, and melanges in accretionary complexes, Eastern Indonesia. The American Association of Petroleum Geologists Bulletin 70, 1729–1741.

Belo, O.A., 1994. Comentários sobre a Geologia da Mina de Ouro Fino—Docegeo internal memorandum.

Belo, O.A., 1994. Projeto Riacho dos Machados, Relatório Final—Docegeo internal report GS-RAS-94-20.

Berthé, D., Choukroune, P., Jegouzo, P., 1979. Orthogneiss, mylonite, and noncoaxial deformation of granites. Journal of Structural Geology 2, 31–42.

Blenkinsop, T.G., 2002. New technologies for analysing ore-body geometry: implications for fluid flow, deformation and mineralization. In: Vearncombe, S., (Ed.), Kalgoorlie, Australian Institute of Geoscientists, Applied Structural Geology for Mineral Exploration and Mining, pp. 15–17.

Brock, W.G., Engelder, T., 1977. Deformation associated with the movement of the Muddy Mountain overthrust in the Buffington Window, southern Nevada. Geological Society of America Bulletin 88, 1667–1677.

Carlson, C.A., 1991. Spatial distribution of ore deposits. Geology 19, 111–114.

Chemale, F., Jr., Alkimim, F.F., Endo, I., 1993. Late Proterozoic Tectonism in the Interior of the Sao Francisco Craton. Hobart, Tasmania, Australia, pp. 29–42.

Chemale, F. Jr, Rosiére, C.A., Endo, I., 1994. The tectonic evolution of the Quadrilátero Ferrífero, Minas Gerais, Brazil. Precambrian Research 65, 25–54.

Costa, J.F.C.L., 1997. Developments in recoverable reserve estimation and ore body modelling. Unpublished Ph.D. dissertation. University of Queensland.

Docegeo, 1992. Mapa geologico e perfís da Mina de Ouro Fino. Docegeo, Brazil.

David, M., 1977. Developments in Geomathematis 2—Geostatistical Ore Reserve Estimation. Elsevier, New York.

Fonseca, E., 1993. Depósito Aurífero de Riacho dos Machados, Minas Gerais: Hidrotermalismo, Deformaçao e Mineralizaçao Associados. Belo Horizonte, Unpublished M.Sc. dissertation. UFMG, Universidade Federal de Minas Gerais.

Gendswill, D.J., Stauffer, M.R., 1981. Analysis of triaxial ellipsoids: their shapes, plane sections, and plane projections. Mathematical Geology 13-2, 135–152.

Guimarães, M.L.V., Crocco-Rodrigues, F.A., Oliveira, O.A.B., Greco, F.M., 1993. Geologia do Bloco Itacambira–Monte Azul entre Barrocao e Porteirinha-MG. 4th Simpósio de Geologia de Minas Gerais 12, 74–78.

Hassard, T.H., 1991. Understanding Biostatistics. Year Boob, Mosby.

Journel, A.G., Huijbregts, C.J., 1978. Mining Geostatistics. Academic Press, London.

Kiang, C.H., Miranda, F.P., Magalhaes, L., Alkimin, F.F., 1988. Consideraçoes sobre a Evoluçao Tectônica da Bacia do Sao Francisco. 35th Congresso Brasileiro de Geologia 5, 2076–2090.

Leymarie, P., 1968. Une méthode permettant de mettre en évidence le caractère ordonné de la distribution de certains gîtes minéraux: application aux gisements du Massif Central français. Mineralium Deposita 3, 334–343.

Lin, S., Williams, P.F., 1992. The geometrical relationship between the

stretching lineation and the movement direction of shear zones. Journal of Structural Geology 14, 491–497.

Lister, G.S., Snoke, A.W., 1984. S–C mylonites. Journal of Structural Geology 14, 617–638.

Machado, N., Schrank, A., Abreu, F.R., Knauer, L.G., Abreu, P.A.A., 1989. Resultados Preliminares da Geocronologia U/Pb na Serra do Espinhaço Meridional. 5th Simpósio de Geologia de Minas Gerais 5, 171–174.

Magalhães, L., 1988. Análise Estrutural Qualitativa nos sedimentos do Grupo Bambuí-Região Sudeste da Bacia do São Francisco (Faixa Sete Lagoas–Serra do Cipó). Universidade Federal de Ouro Preto, Ouro Preto.

Mandelbrot, B.B., 1982. The Fractal Geometry of Nature. Freeman, San Francisco.

Marshak, S., Alkimin, F., 1989. Proterozoic contraction/extension tectonics of the Southern Sao Francisco region, Minas Gerais, Brazil. Tectonics 8, 555–571.

Mascarenhas, J.F., Misi, A., Motta, A.C., Sá, J.H.S., 1984. Província do Sao Francisco, 46–122.

Matheron, G., 1963. Principles of geostatistics. Economic Geology 58, 1246–1266.

Matsumura, S., 1981. Three-dimensional expression of seismic particle motions by the trajectory ellipsoid and its application to the seismic data observed in the Kanto District, Japan. Journal of Physics of the Earth 29, 221–239.

Milton, N.J., 1980. Determination of the strain ellipsoid from measurements on any three sections. Tectonophysics 64, 19–27.

Monteiro, R.N., 1989. Mina de Ouro Fino-MG, Relatório de Viagem—01. Belo Horizonte-MG.

Monteiro, R.N., 1993. Proposta para a Análise Estrutural Variográfica da Mina de Ouro Fino.

Monteiro, R.N., 1996. Gold mineralization at Ouro Fino Mine, Brazil: structure and alteration. Unpublished Ph.D. dissertation. The University of Western Ontario, London, Ontario, Canada.

Newton, P.G.N., 2000. The integration of structural geology and directional variography at three orogenic gold deposits: implications for orebody geometry and mine practice. Abstract of a Ph.D. dissertation, University of Western Australia.

Newton, P.G.N., Ridley, J.R., Groves, D.I., Khosrowshahi, S., Smith, B., 1997. Integration of directional variography and structural geology: an example from the Santa-Craze BIB-hosted Au deposit, near Kalgoorlie, Western Australia. Chronique de la Recherche Miniere 529, 105–125.

Olea, R.A., Christakos, G., Clark, I., David, M., Journel, A.G., Krige, D.G., 1991. Geostatistical Glossary and Multilingual Dictionary. Oxford University Press, New York, USA.

Pedrosa-Soares, A.C., Noce, C.M., Vidal, P., Monteiro, R.L.B.P., Leonardos, O.H., 1992. Toward a new tectonic model for the Late Proterozoic Araçuaí (SE Brazil)–West Congolian (SW Africa) Belt. Journal of South American Earth Sciences 6 (1/2), 33–47.

Pedrosa-Soares, A.C., Noce, C.M., Vidal, P., Leonardos, O.H., Lobato, L., Carvalho, C.T., Magni, M.C.V., Faria, L.F., 1992. Novo Modelo Evolutivo para a Faixa Araçuaí: Dados Complementares e Síntese. 37th Congresso Brasileiro de Geologia 1, 287–288.

Pflug, R., Renger, F., 1973. Estratigrafia e Evoluçao Geológica da Margem SE do Craton Saofraciscano. 27th Congresso Brasileiro de Geologia 2, 5–19.

Powell, C.M., 1969. Intrusive sandstone dykes in the Siamo Slate near Negaunee, Michigan. Geological Society of America Bulletin 80, 2585–2594.

Ramsay, J.G., Huber, M.I., 1983. The Techniques of Modern Structural Geology: Strain Analysis. Academic Press, London.

Schöll, W.U., Fogaça, A.C.C., 1979. Estratigrafia da Serra do Espinhaço. 1st Simpósio de Geologia de Minas Gerais 1, 55–73.

Siga, O. Jr, Cordani, U., Kawashita, K., Basei, M.A.S., Taylor, P.N., 1987. Aplicaçao dos Isótoposde Sr e Pb nas Rochas Gnáissico—Migmatíticas de Itacambira-Barrocao. 4th Simpósio de Geologia de Minas Gerais 4, 45–57.

Siga, O. Jr, Cordani, U.G., Basei, M.A.S., Teixeira, W., Kawashita, K., Schmus, R.V., 1987. Contribuiçao ao Estudo Geológico-geocronológico da Porçao Nordeste de Minas Gerais. 4th Simpósio de Geologia de Minas Gerais 4, 29–44.

StatSoft, 1998. Statistica™ for Windows™. StatSoft Inc.

Uhlein, A., Pedreira, A.J., Trompette, R.R., 1992. Evoluçao Geológica da Faixa Móvel Espinhaço nos Estados de Minas Gerais e Bahia. 37th Congresso Brasileiro de Geologia 1, 290–291.

Vearncombe, J., Vearncombe, S., 1999. The spatial distribution of mineralization: applications of Fry Analysis. Economic Geology 94, 75–486.

Winslow, M.A., 1983. Clastic dike swarms and the structural evolution of the foreland fold and thrust belt of the southern Andes. Geological Society of America Bulletin 94, 1073–1080.